Mechanism of Terahertz Electromagnetic Wave from Intrinsic Josephson Junctions

doi: 10.1103/PhysRevLett.102.127002

Mechanism of Terahertz Electromagnetic Wave Emission from Intrinsic Josephson Junctions

Masashi Tachiki,[1] Shouta Fukuya,[2] and Tomio Koyama[3]

[1]*Graduate school of Frontier Science, The University of Tokyo, 5-1-6 Kashiwanoha, Kashiwa 277-8581, Japan*
[2]*Institute for Solid State Physics, University of Tokyo, Kashiwa, Chiba 277-8581, Japan*
[3]*Institute for Materials Research, Tohoku University, Katahira 2-1-1, Aoba-ku, Sendai 980-77, Japan*

(Received 29 October 2008; published 25 March 2009)

Using a 3D parallelepiped model of the stack of intrinsic Josephson junctions, we calculate the cavity resonance modes of Josephson plasma waves excited by external electric currents. The cavity modes accompanied by static phase kinks of the order parameter have been intensively investigated. Our calculation shows that the kink phase state is unfavorable, since the static phase kinks reduce the order parameter amplitude and thus the superconducting condensation energy. We point out that the oscillating magnetic field of the cavity mode penetrates the vacuum from the sample surfaces and the energy of the magnetic field plays an important role to determine the orientation of the cavity resonance mode. On the basis of the above discussions, we calculate the *I-V* characteristic curve, the THz wave emission intensity and the other physical quantities.

DOI: 10.1103/PhysRevLett.102.127002 PACS numbers: 74.50.+r, 74.25.Gz, 85.25.Cp

Emission of terahertz electromagnetic (em) waves from intrinsic Josephson junctions (IJJ) in high temperature superconductors has been extensively studied [1–8]. Recently, Ozyuzer *et al.* succeeded in detecting strong and continuous emission of terahertz em waves from mesa-shaped samples of the high temperature superconductor $Bi_2Sr_2CaCu_2O_8$ (BSCCO) [9]. The general mechanism for the emission is as follows. When an external current is applied along the c axis, the ac Josephson current in the resistive state excites a cavity resonance mode of Josephson plasma wave in the sample. The excited standing wave of Josephson plasma is converted to a terahertz em wave at the mesa surfaces and the em wave is emitted into the vacuum space. However, details of the mechanism have not yet been clarified, although it is important for designing the terahertz em wave emitters with use of IJJ.

Recently, Hu and Lin [10,11], and Koshelev [12] proposed the following new mechanism. When the inductive interaction between the superconducting CuO_2 layers in BSCCO is strong, static kink structures arise in the phase difference of superconducting order parameter between the superconducting layers. The phase kinks induce cavity resonance modes of the Josephson plasma. This is a new dynamic state caused by the nonlinear effect special in the IJJ system. In this Letter, we first discuss the stability of this new state, and then we investigate the mechanism of the terahertz em wave emission on the basis of the discussion.

For the sample of IJJ, we use a model shown in Fig. 1. In this figure the superconducting CuO_2 layers and the insulating layers in the IJJ are shown in green and light green, respectively. An external electric current is applied in the direction of the z axis, perpendicular to the layers. The L_x, L_y, and L_z are the sample lengths, respectively, along the x, y, and z axes. Now, we derive the equation for the simulation. The superconducting order parameter of the lth layer is expressed as $\Psi_l = \Delta_l(\boldsymbol{r}, t)\exp[i\varphi_l(\boldsymbol{r}, t)]$ with $\boldsymbol{r} = (x, y)$, x, y and t referring to the spatial and temporal coordinates, respectively. We assume that the amplitude $\Delta_l(\boldsymbol{r}, t)$ is constant independent of space and time, and only the phase $\varphi_l(\boldsymbol{r}, t)$ is dependent on space and time. In this case, the current density along the z axis is given by a sum of the Josephson, quasiparticle, and displacement current densities as

$$I_{l+1,l} = J_c \sin\psi_{l+1,l} + \sigma_c E_{z,l+1,l} + \frac{\epsilon}{4\pi}\partial_t E_{z,l+1,l}, \quad (1)$$

where J_c is the critical current density, σ_c is the normal conductivity along the c axis, and $E_{z,l+1,l}$ is the electric field between $(l+1)$th and lth layer along the z axis. In Eq. (1), $\psi_{l+1,l}(\boldsymbol{r}, t)$ is the gauge invariant phase difference defined as

$$\psi_{l+1,l}(\boldsymbol{r}, t) = \varphi_{l+1}(\boldsymbol{r}, t) - \varphi_l(\boldsymbol{r}, t) - \frac{2\pi}{\phi_0} \times \int_{z_l}^{z_{l+1}} A_z(\boldsymbol{r}, z, t)dz, \quad (2)$$

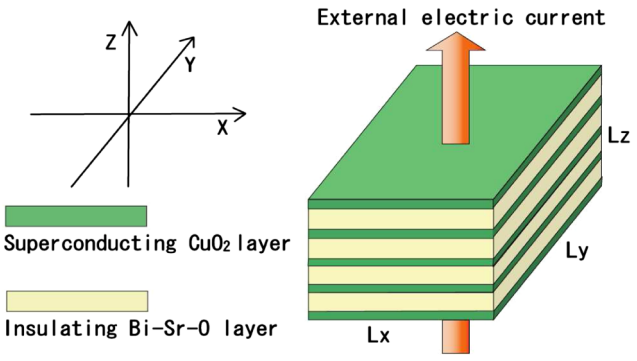

FIG. 1 (color online). Schematic view of intrinsic Josephson junctions.

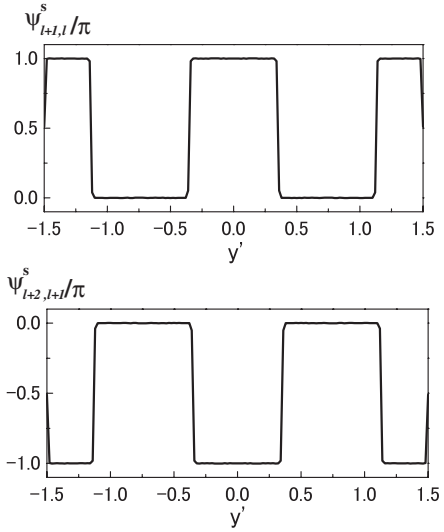

FIG. 2. Typical configuration of the static phase difference.

with the vector potential $A_z(\boldsymbol{r}, z, t)$ and the flux unit ϕ_0. For the superconducting current density in the CuO_2 plane, we use the generalized London equations, since the Ginzburg-Landau parameter is very large in BSCCO. We insert Eqs. (1) and (2) into Maxwell's equations along with the superconducting current in the CuO_2 layers. Following the calculation procedure given in [6], we have

$$\partial^2_{x'}\psi_{l+1,l} + \partial^2_{y'}\psi_{l+1,l} = (1-\zeta\Delta^{(2)})(\sin\psi_{l+1,l} + \beta\partial_{t'}\psi_{l+1,l} + \partial^2_{t'}\psi_{l+1,l}). \quad (3)$$

In above equation, we use normalized units for length and time, respectively, defined as $x' = x/\lambda_c$, $y' = y/\lambda_c$, $t' = \omega_p t$, where ω_p is the plasma angular frequency, and λ_c is the penetration depth of the magnetic field applied along the x or y axis from the xz or yz surface. The parameters in Eq. (3) are defined as $\zeta = \lambda^2_{ab}/sd$ and $\beta = 4\pi\lambda_c\sigma_c/\sqrt{\epsilon_c}$, where the s and d are the thicknesses of the superconducting and insulating layers, respectively. λ_{ab} is the magnetic field penetration depth from the xy-plane surface and ζ is the inductive constant between the CuO_2 layers. The operator $\Delta^{(2)}$ is defined as $\Delta^{(2)} f_l = f_{l+1} - 2f_l + f_{l-1}$. In Eq. (3), we neglect the charging effect in the CuO_2 layers, since we consider the region above the retrapping point, and in this region the charging effect is much weaker than the inductive effect between the CuO_2 layers. Keeping in mind that the IJJ is $Bi_2Sr_2CaCu_2O_8$, we choose $\lambda_{ab} = 0.4\ \mu$m, $\lambda_c = 50 \sim 150\ \mu$m, $s = 3$ Å, $d = 12$ Å, $\beta = 0.02$, and $\zeta = 5 \times 10^5$.

We express the phase difference $\psi_{l+1,l}(\boldsymbol{r}, t)$ as

$$\psi_{l+1,l}(\boldsymbol{r}', t') = \omega_J t' + \psi^t_{l+1,l}(\boldsymbol{r}', t') + \psi^s_{l+1,l}(\boldsymbol{r}') + \frac{I'}{4}\boldsymbol{r}'\cdot\boldsymbol{r}'. \quad (4)$$

The first term in the right-hand side of Eq. (4) is the phase difference due to the ac Josephson effect, the second term is the phase difference due to the excited cavity mode, the third term is a static phase difference, and the fourth term is the phase difference due to an external current density I' normalized by J_c.

The sample lengths L'_x, L'_y, and L'_z which are normalized by λ_c are taken to be 1, 3, and 0.01, respectively. Although the samples used in the experiments [9] is composed of several hundreds of intrinsic Josephson junctions, to simplify the calculation we impose an assumption that the phase difference has a four junctions periodicity along the z axis. Since the sample length along the z axis is much shorter than the wave length of terahertz em wave, the em waves emitted from the side surfaces of the sample are not plane waves. The boundary condition in this case has been given by Bulaevskii and Koshelev [13]. We use the boundary condition and tentatively take $B_x/E_z = \gamma = \pm 0.1$ at the xz surfaces and $B_y/E_z = \gamma = \pm 0.1$ at the yz-surfaces, E_z, B_x and B_y being, respectively, the oscillating parts of electric and magnetic fields at the sample surfaces. Under the boundary condition, we numerically solved Eq. (3) and obtained a solution of the static phase difference $\psi^s_{l+1,l}(\boldsymbol{r})$ with a kink and antikink structure at a cavity resonance voltage $V' = 3.96$ as shown in Fig. 2. The normalized voltage V' is defined by V/V_p, V and V_p being the voltages between the CuO_2 layers and $\hbar\omega_p/2e$, respectively. As seen in the figure, the kink phase structure occurs along the y axis. The oscillating electric field of the cavity mode at a time is shown in Fig. 3(a). The electric field E_z is almost uniform along the x axis, and the electric field along the y axis is a standing wave with two wave lengths. The amplitude of the oscillating electric field is symmetric with respect to the center of the sample along the x and y axes. The electric field pattern of cavity mode in Fig. 3(a) seems to be consistent with the electric field distribution recently observed by Wang *et al.*, using low temperature scaning laser microscopy [14]. The oscillating magnetic fields B_x and B_y at the time is shown in Fig. 3(b) and 3(c). The absolute value of B_x is much larger than that of B_y inside

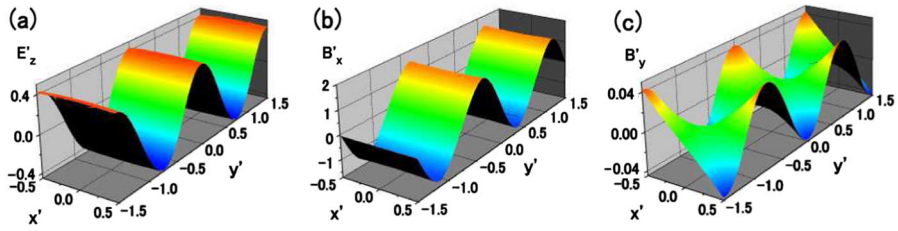

FIG. 3 (color online). Snapshot of the electric and magnetic fields at $V' = 3.96$ and $I' = 0.106$. E'_z, B'_x, and B'_y are electric and magnetic fields normalized by $\phi_0/2\pi\lambda_c d$. The sample with the lengths $L'_x = 1$, $L'_y = 3$, and $L'_z = 0.01$ are used.

the sample and at the yz surfaces. This state with phase kinks is similar to those obtained by Hu and Lin [10,11], and Koshelev [12]. In the above calculation, when we took several kinds of the initial condition with modulations along the z axis for the phase difference $\psi_{l+1,l}(\boldsymbol{r}, t)$, we obtained the two types of phase kink state. The internal energies of the phase kink states consist of superconducting current energies and electric and magnetic energies. The internal energies have almost the same value in independence of the initial conditions. If we took an initial condition that the phase difference is perfectly uniform along the z axis, we obtained a solution of the state without phase kink in place of the solutions with phase kinks. The calculated internal energies of the phase kink states are lower than that of the state without phase kink, and the ratio of the energy of the phase kink state to the energy of the state without phase kink is about 0.8.

The kinks of the phase difference in Fig. 2 cause the π-kinks in the CuO_2 layers and the π-kinks reduce the amplitude of superconducting order parameter around the kinks. The cause of the reduction of the order parameter amplitude is similar to that in the vortex core of the Abrikosov vortex. The reduction of the amplitude decreases the superconducting condensation energy. Using one dimensional model along the y axis and the Ginzburg-Landau equation (GL eq.), we estimate the decrease of the condensation energy due to the kinks in the following way. From GL eq. we obtain the coupled equations for the amplitude Δ and phase φ: $\partial_y^2\Delta - \Delta(\partial_y\varphi)^2 + \Delta - (\Delta^3/\Delta_0^2) = 0$ and $2\partial_y\Delta\partial_y\varphi + \Delta\partial_y^2\varphi = 0$. The y axis is normalized by the coherence length ξ, and Δ_0 is the amplitude of the order parameter without kink. We use a linear approximation for φ inside the kink with the width y_0 and express $\varphi = (\pi/y_0)y$, y taking the values from 0 to y_0. The value of y_0 is approximately equal to $\lambda_c/(\xi\sqrt{\zeta})$. Under the condition, the coupled equations give the relation $(\partial_y\varphi)^2 = 1 - (\Delta/\Delta_0)^2$ inside the kink. Using this relation we calculate the decrease of the condensation energy due to the kinks from the formula $E_c = (H_c^2/8\pi) \times \int[1 - (\Delta/\Delta_0)^2]dV$, H_c being the thermodynamic critical field. For the estimation of value of E_c, we use the values $H_c = 1$ T, $\xi = 50$ Å, $\zeta = 5 \times 10^5$, and $\lambda_c = 100$ μm. Then, if we add E_c to the internal energy of the kink phase, we obtain that the total energy of the kink state is $2 \sim 3$ times larger than the internal energy of the state without kink. Therefore, the state with phase kinks is unfavorable for the state without kink.

In the calculation of the resonance mode shown in Fig. 3, we have missed an important fact. As shown in Fig. 3 the magnitude of B_x is much larger than that of B_y at the yz surfaces. Although the oscillating magnetic field B_x does not contributes to the radiation, it penetrates the vacuum from the surface. We should add this magnetic energy in the vacuum to the internal energy of the state. If the resonance occurs along the x axis instead of along the y axis, the magnitude of B_y becomes much larger than that of B_x. Since the xz surface area is narrower than the yz surface area for the sample, the magnetic energy penetrated from the xz surface into the vacuum is smaller, and thus stabilizes the magnetic field $\boldsymbol{B}$ along the y axis. Therefore, the cavity resonance mode occurs along the x axis rather than along the y axis in the sample [9]. The origin of the magnetic energy stabilizing $\boldsymbol{B}$ along the y axis in this case is similar to that of the shape anisotropy energy of a ferromagnet that stabilizes its magnetization along the longer size direction of the ferromagnet.

On the basis of these discussions, we investigate the physical properties originating from the cavity resonance along the x axis in the states without phase kink. In the following calculation, we assume that the magnetic field $\boldsymbol{B}$ is parallel to the y axis as is discussed above, and use the boundary condition $B_y/E_z = \gamma = 0.1$ at the yz surfaces. Figure 4(a) shows the calculated current-voltage (I-V) curve for $L_x' = 2$. As seen in the figure, two sharp peaks appear, respectively, at the normalized voltages $V' = 2.9$ and 6.2. These sharp peaks are caused by the cavity resonance of the excited electric and magnetic fields in the sample. Since the amplitude of the oscillating electric field is large at the resonance voltages, the sharp peaks are considered to be internal Shapiro steps induced by the oscillating electric fields in a self-consistent way [15]. Figure. 4(b) shows the current-voltage curve for $L_x' = 3$. The cavity resonance voltage at $V' = 1.7$ almost coincides with the retrapping voltage [9]. The sharp resonance peaks have not been observed in the experimental current-voltage characteristics in large BSCCO mesas. This discrepancy may come from the fact that heating effect is not included in the present theory. A snapshot of the oscillating electric and magnetic fields for $L_x' = 2$ and at $V' = 2.9$ is shown in Fig. 5(a). The amplitudes of both the electric and magnetic fields are asymmetric with respect to the center of the sample. Figure 5(b) shows the emission intensities (the time averages of the Poynting vectors) for the boundary condition parameters $\gamma = 0.1$ and $\gamma = 1$ as functions of V'. The black circles indicate the emission intensities for

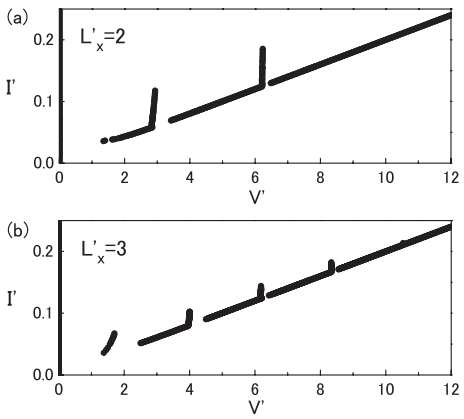

FIG. 4. I-V curves in the two cases of (a) $L_x' = 2$ and (b) $L_x' = 3$.

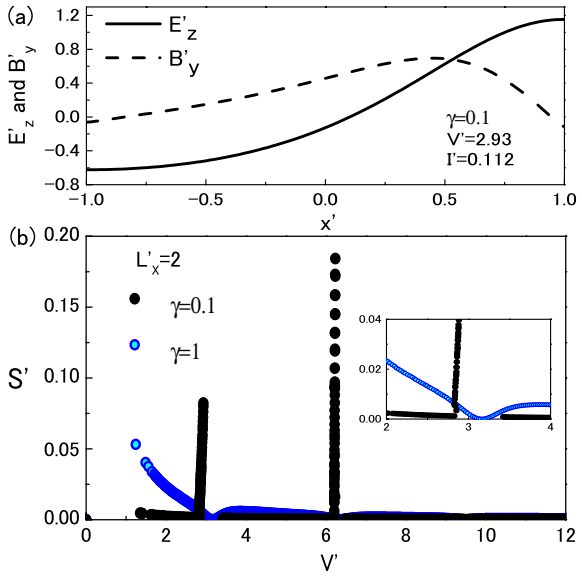

FIG. 5 (color online). (a) Snapshot of the electric and magnetic fields at the top of first internal shapiro step $V' = 2.93$ and $I' = 0.112$. The normalization of E'_z and B'_y is the same as that in Fig. 3. (b) Voltage dependence of the intensity of emission from intrinsic Josephson junctions. The length of the sample is $L'_x = 2$. Black circles and blue circles show the emission intensities in the cases of $\gamma = 0.1$ and $\gamma = 1$, respectively. The time average of Poynting vector S' is normalized by $c(\phi_0/2\pi\lambda_c d)^2/4\pi$.

$\gamma = 0.1$. The sharp emission peaks appear at the cavity resonance voltages as seen in Fig. 4(a). The maximum emission power at $V' = 2.9$ is estimated to be 23 mW for the sample with $L'_x = 2$, $L'_y = 3$, $L'_z = 0.01$, and $\lambda_c = 100\ \mu$m. The blue circles in Fig. 5(b) show the emission intensities for the boundary condition parameter $\gamma = 1$. The $\gamma = 1$ indicates that B_y/E_z is equal to ± 1 at the yz surfaces, and the boundary condition is that for the emitted em wave being plane wave. The plane wave emission occurs when L_y and L_z are much longer than the wave length of the emitted em wave. As seen in the figure, the voltage dependence of the emission intensity for $\gamma = 1$ is very different from that for $\gamma = 0.1$ and the intensity vanishes at the cavity resonance voltages. Matsumoto *et al.* have calculated the intensity in this case and shown that the oscillating electric and magnetic fields vanish at the yz surfaces [16]. The results indicate that the emission intensity strongly depends on the sample size relative to the em wave length. Each of the blue circles in Fig. 6 denotes the lowest normalized voltage V' or the lowest normalized frequency of the cavity resonance for each of 7 samples with different L'_x. As seen in the figure, the blue circles are on a line.

The conclusion of this Letter is as follows. The cavity resonance state with the static phase kinks is unfavorable, since the phase kinks reduce the order parameter amplitude around the kinks and thus the superconducting condensation energy. Nonradiative component of the oscillating magnetic field of the cavity resonance mode plays an important role to determine the orientations of the cavity resonance modes. The orientation is closely connected with the sample shape. In the I-V characteristic curve, sharp peaks appear at the cavity resonance. At the resonance, sizable powers of the continuous and coherent terahertz wave emission were obtained.

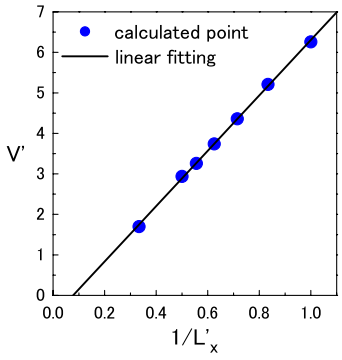

FIG. 6 (color online). $1/L'_x$ dependence of the first resonance voltage. The solid line represents the linear fitting. L'_y is taken to be 3.

The authors thank X. Hu, A. Koshelev, L. Bulaevskii, M. Matsumoto, M. Machida, S. Lin, K. Kadowaki, U. Welp, K. E. Gray, L. Ozyuzer, W. K. Kwok, C. Kurter, and H. B. Wang for valuable discussions. One of the authors (M. T.) thanks H. Koinuma, H. Takagi, K. Ito, and K. Itaka for great support to this research. This work has been supported by the JST (Japan Science and Technology Agency) CREST project and by the CTC (Core-to-Core) program.

[1] R. Kleiner, F. Steinmeyer, G. Kunkel, and P. Müller, Phys. Rev. Lett. **68**, 2394 (1992).
[2] S. Sakai, P. Bodin, and N. F. Pedersen, J. Appl. Phys. **73**, 2411 (1993).
[3] T. Koyama and M. Tachiki, Solid State Commun. **96**, 367 (1995).
[4] Y. Matsuda *et al.*, Phys. Rev. Lett. **75**, 4512 (1995).
[5] K. Lee *et al.*, Phys. Rev. B **61**, 3616 (2000).
[6] M. Tachiki, M. Iizuka, S. Tejima, and H. Nakamura, Phys. Rev. B **71**, 134515 (2005).
[7] K. Kadowaki *et al.*, Physica (Amsterdam) **437C**, 111 (2006).
[8] M.-H. Bae, H.-J. Lee, and J.-H. Choi, Phys. Rev. Lett. **98**, 027002 (2007).
[9] L. Ozyuzer *et al.*, Science **318**, 1291 (2007).
[10] S. Lin and X. Hu, Phys. Rev. Lett. **100**, 247006 (2008).
[11] X. Hu and S. Lin, Phys. Rev. B **78**, 134510 (2008).
[12] A. E. Koshelev, Phys. Rev. B **78**, 174509 (2008).
[13] L. N. Bulaevskii and A. E. Koshelev, J. Supercond. Novel Magnetism **19**, 349 (2006).
[14] H. B. Wang *et al.*, arXiv:0807.2749.
[15] H. B. Wang, P. H. Wu, and T. Yamashita, Phys. Rev. Lett. **87**, 107002 (2001).
[16] H. Matsumoto, T. Koyama, and M. Machida, Physica (Amsterdam) **468C**, 654 (2008).